Near Atomic Scale Studies of Electronic Structure at Grain Boundaries in Ni_3Al

David A. Muller,[1] Shanthi Subramanian,[2] Philip E. Batson,[3] Stephen L. Sass,[2] and John Silcox[1]
[1]*School of Applied and Engineering Physics, Cornell University, Ithaca, New York 14853*
[2]*Department of Materials Science and Engineering, Cornell University, Ithaca, New York 14853*
[3]*IBM Thomas J. Watson Research Center, Yorktown Heights, New York*
(Received 19 June 1995)

Why does boron doping improve the room temperature ductility of polycrystalline Ni_3Al? Besides preventing environmental embrittlement, B changes the fracture mode from intergranular to transgranular, suggesting an increase in the cohesive strength of the grain boundaries. This change in bonding at the grain boundary has been measured using spatially resolved electron energy loss spectroscopy. The Ni $L_{2,3}$ core edge, which is sensitive to the filling of the Ni d band, shows that only the B-rich regions of the grain boundary have a bonding similar to that of the bulk material. These changes suggest a simple model to describe the cohesion of the boundary.

PACS numbers: 61.72.Mm, 61.66.Dk, 62.20.Mk, 71.25.Pi

There is an intimate relationship between the electronic structure and the mechanical properties of a material. Change one, and the other must change too. In this Letter, that relationship is traced for the prototypical high temperature intermetallic compound Ni_3Al. Stoichiometric Ni_3Al is ductile as a single crystal, but it exhibits brittle intergranular fracture when polycrystalline. In contrast, Ni-rich (e.g., $Ni_{0.76}Al_{0.24}$) polycrystals doped with boron and appropriately heat treated are found to be ductile and to fail transgranularly [1,2]. In this case, it is suspected that the cohesion of the grain boundaries, which contain boron and extra nickel [2], has increased relative to that in the undoped polycrystal stoichiometric compound. The central issue is *how is the increased cohesion reflected in bonding changes at the boundary?* To answer this question, electron energy loss spectroscopy (EELS) at 100 keV with a finely focused electron beam (2 to 5 Å lateral resolution [3–5]) is used. We report studies of the Ni $L_{2,3}$ edges (sensitive to the filling of the Ni d band) at boundaries in B-doped and undoped material in comparison with bulk material. B-rich regions of boundaries have an electronic structure comparable to the bulk material whereas significant differences are seen for undoped regions. Simple bond order models are used to relate these to changes in cohesion at the boundaries and suggest a natural explanation for the observed mechanical properties.

Auger electron spectroscopy [2] identifies Ni enrichment and B segregation at the grain boundaries. The B results are confirmed by field ion microscopy [6,7] which also suggests fluctuations in B concentration along the boundary. Ni segregation is confined within one or two planes of the boundary in arc cast and homogenized material [8,9], consistent with embedded atom method (EAM) simulations [10,11]. In undoped Ni_3Al the boundaries are not intrinsically brittle but can exhibit some ductility when heat treated and tested in a clean environment [12]. Moisture induced embrittlement has also been demonstrated in polycrystalline Ni_3Al [13]. However, the fracture mode in undoped material is always intergranular, irrespective of the environment. B doping improves the ductility at ambient temperatures and will suppress the intergranular failure in the Ni-rich material suggesting that the boundary is no longer the weak link. Thus, the question noted above can be refined in this case to ask: *how does boron strengthen the Ni-rich boundary?*

Experimentally we use a scanning transmission electron microscope (STEM) to pass a 100 keV electron beam (3 to 5 Å diameter) through a thin (400 Å) specimen containing a grain boundary oriented so the beam direction is parallel to the boundary plane. If the beam is placed on the boundary, probe electrons scatter wholly in the internal interface and the local density of states (LDOS) of the internal interface (not a free surface) is measured. The choice of film thickness is a compromise between minimizing the contribution from surface states ($\gg$20 Å thick) and beam broadening due to multiple elastic scattering ($<$500 Å for subnanometer resolution [14]). The Ni L edges (L_2:$2p_{1/2} \rightarrow 3d_{3/2}$ and L_3:$2p_{3/2} \rightarrow 3d_{3/2}, 3d_{5/2}$) at 870 and 853 eV energy loss, respectively, select excitations from the Ni $2p$ core orbitals to states above the Fermi level on the same Ni site. Figure 1 shows L edges from various Ni-Al alloys after background subtraction and deconvolution of multiple scattering (scaled to the Hartree-Slater cross section for a Ni atom [15]).

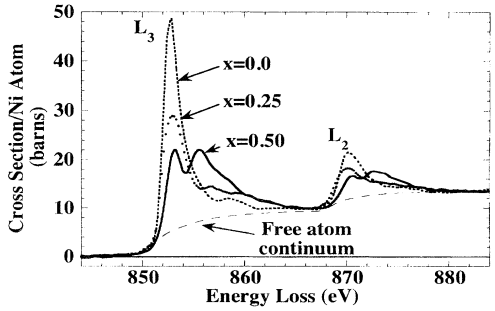

FIG. 1. Measured Ni $L_{2,3}$ edge for the $Ni_{(1-x)}Al_x$ system showing the decrease in the sharp peak ("white line") at the onset of the L_2 and L_3 edges with increasing Al concentration.

 0031-9007/95/75(26)/4744(4)$06.00

From Fermi's golden rule and dipole selection rules, the observed intensity is proportional to the LDOS with s-like ($l = 0$) or d-like ($l = 2$) symmetry in the conduction band, and transitions to $l = 2$ states dominating by a factor of ~100 [16–19]. The overlap of the final state with the very localized $2p$ initial state defines the measured LDOS to be proportional to a muffin tin projected DOS (and differing from it only by a matrix element that is slowly varying with energy [19]). Consequently the measured number of "d holes" in Ni is the muffin tin value of 1.4 [20,21] instead of the 0.6 expected for atomic d orbitals. The area under the sharp peaks at the onset of the Ni L_2 and L_3 edges is proportional to the number of holes in the "unhybridized" Ni d band, $h_d = 10 - n_d$ [18], and is seen to decrease as the alloy becomes increasingly Al rich. The absence of a core level shift between Ni and Ni_3Al suggests little net charge is transferred to the Ni site and the apparent Ni d-band filling takes place by hybridization with the Al s, p electrons. *Ab initio* calculations [20] show the conduction band of the Ni-Al alloys follows the traditional picture [22] of a sharply peaked d resonance on the Ni site mixing with a broad free-electron-like band common to both the Ni and Al sites. As Ni-Ni neighbors are replaced with Ni-Al, the Ni d resonance is increasingly hybridized with $l = 2$ component of the free electron band. This shifts states away from the main d band to its tails [21], resulting in a decrease in DOS at the Fermi level and changes the shape of the measured EELS spectra (Fig. 1) from sharply peaked at the onset to lower and broader. The more strongly hybridized alloys tend to have larger heats of formation and stiffer elastic constants [20].

A VG HB 501 STEM modified to achieve high spatial (drift <0.05 nm/min) and energy (drift <0.02 eV/min) stability was used to obtain the EELS data as well as to carry out microscopy and microanalysis. Grain boundaries in polycrystalline $Ni_{0.76}Al_{0.24}$ with and without boron were examined. Details of specimen preparation and the techniques used for limiting radiation damage are given elsewhere [23] as are the results of energy dispersive x-ray analysis (EDX) [24].

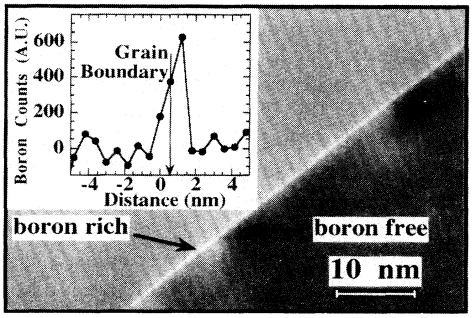

FIG. 2. ADF image of a large-angle grain boundary in B-doped $Ni_{0.76}Al_{0.24}$ (footnote a of Table I). The boundary appears bright due to Ni enrichment. B is present at parts of the boundary which show strain contrast (light). Dark regions have no detectable B. Inset is a EELS B-K edge line scan across the boundary showing B segregation to the boundary.

Ni segregation to the boundaries was observed both in the presence and in the absence of B. From annular dark field (ADF) images, where the boundaries were viewed edge on, the Ni-rich region of the large angle boundaries was estimated to be only 0.5–0.8 nm wide. The boundaries were tilted a few mrad away from edge-on orientations to perform the EELS measurements in order to limit the probe dechanneling which was found to occur for strongly diffracting conditions. This broadened the projected width of the boundaries by 0.2–0.4 nm so the spatial resolution is subnanometer but not atomic. The ADF signal, recorded simultaneously with the EELS signal, was used to locate the center of the boundary and as a common reference map for placing the probe to record

TABLE I. Measured d hole trends and estimated boundary energies γ_B. The error bars for γ_B are for the uncertainty in the EELS measurements. See text for additional systematic errors. LA = large angle.

Bulk composition	Boundary character	B layers at boundary	Number of d holes per Ni atom	γ_B (mJ/m^2)
Ni	**Bulk**		**1.44**	
$Ni_{0.76}Al_{0.24}B_{0.001}$	LA[a]	<0.01	1.32 ± 0.04	1365 ± 80
$Ni_{0.76}Al_{0.24}$	LA[b]		1.29 ± 0.06	1213 ± 80
$Ni_{0.76}Al_{0.24}B_{0.0005}$	LA[c]	<0.02	1.16 ± 0.05	556 ± 150
$Ni_{0.76}Al_{0.24}$	3.5° Tilt[d]			
$Ni_{0.76}Al_{0.24}B_{0.0005}$	3.0° Tilt[d]	<0.01		
$Ni_{0.76}Al_{0.24}B_{0.0005}$	LA[c]	0.05 ± 0.03	1.09 ± 0.05	202 ± 200
Ni_3Al	**Bulk**		1.05 ± 0.08	
$Ni_{0.76}Al_{0.24}B_{0.0001}$	LA[a]	0.14 ± 0.06	1.01 ± 0.04	−200 ± 200
NiAl	**Bulk**		0.6 ± 0.12	

[a] $[\bar{1}21]$ boundary normal, (15 ± 5)° rotation about $[3\bar{1}2]$.
[b] $[\bar{1}10]$ boundary normal, (60 ± 5)° rotation about $[\bar{2}12]$.
[c] $(3\bar{2}0)$ boundary plane, rotated 8° with axis (15 ± 5)° from [100].
[d] Antiphase boundary (APB) at [001] (110) tilt boundary.

the B and Ni EELS edges. B segregation to the boundary was detected using EELS (Fig. 2). These results indicate that the specimens used here are comparable with those in earlier studies [2,6–9]. The interesting result of Fig. 2 ($Ni_{0.76}Al_{0.24}$ doped with 1000 ppm B) is that the boron segregation along that grain boundary is not uniform. This is atypical; our measurements on other boundaries [24] suggest B is uniformly present or absent (see Table I). However, this boundary (Fig. 2) provides a convenient demonstration of the effect of B on the Ni bonding at the same grain boundary. Figure 3 shows the Ni L_3 edge recorded at the B-rich and B-poor regions marked on Fig. 2 and compared with bulk Ni_3Al. In the absence of boron, the Ni d band is less hybridized than the bulk material and comparison to Fig. 1 shows it is similar to pure Ni. However, in regions where a substantial B signal could be detected, the Ni was at least as strongly hybridized as the bulk and possibly a little more. The same trends are seen at a variety of grain boundaries (Table I): *when B is present at a Ni-rich grain boundary, the Ni d DOS resembles that of bulk Ni_3Al; when no B is detected at a Ni-rich grain boundary, the Ni d DOS is closer to that of bulk Ni (more d holes and a larger DOS at the Fermi level).*

The loss of hybridization at the boundary will reduce the cohesive energy, change the elastic constants (probably lower), and, because the bonds are less saturated, increase the chemical reactivity of the boundary. The ordering trends in these alloys have also been discussed in terms of the strong s, p-d hybridization between Ni and Al [25]. By relating the moments of the LDOS to the local atomic environment, bond order potentials provide a controlled approximation for working back from the measured electronic structure to physical properties. In transition metals, the cohesive energy, bulk modulus, and structure can be predicted from the filling of the d band [22] (see [26] for a modern review). Such ideas describe the trends in the heat of formation, ΔH, for the d block-aluminum alloys [27]. A similar model, corrected to satisfy the experimentally observed local charge neutrality, is used here to estimate the boundary energies.

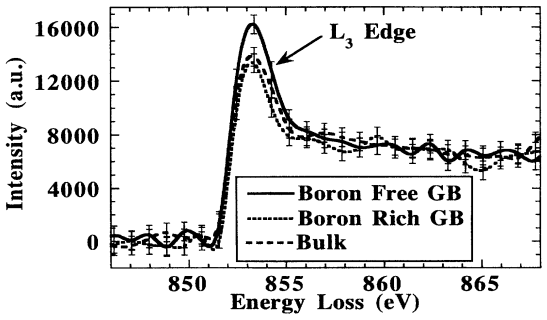

FIG. 3. Ni L_3 edge recorded at B-rich and B-free regions of the boundary shown in Fig. 2. A spectrum taken well away from the boundary is shown as bulk Ni_3Al. All spectra were recorded within minutes of each other, under the same illumination conditions and specimen tilt. Only the probe position was changed. Similar trends were seen using the Ni L_2 edge.

As we are interested in small energy differences rather than absolute energies, we use the force theorem [28] with tight binding eigenvalues to describe the alloy heats of formation, ΔH. The dominant contribution to the change in cohesive energy is then the bond energy

$$E_{\text{bond}} = \sum_i \int_{-\infty}^{E_{\text{Fermi}}} (E - \epsilon_i) d_i(E)\, dE\,, \qquad (1)$$

where $d_i(E)$ is the LDOS on site i with center of gravity ϵ_i [26]. This states that filling bonding states ($E < \epsilon_i$) lowers the energy relative to a free atom with eigenvalue ϵ_i and filling antibonding states ($E > \epsilon_i$) weakens the bond [26]. Thus the strongest bond is for an exactly half filled DOS. Keeping only the second moment of $d_i(E)$, Friedel's model of cohesion for transition metals gives $E_{\text{bond}} = -[An_d(10 - n_d) + Bn_d]$ [22]. The first term comes from using a d band of rms width $W = 20$ Å in Eq. (1) and the second is attributed to s-d hybridization with $B \approx 0.25$ eV. For an almost full d band ($n_d \gtrsim 9$ as in Cu and the Ni-Al alloys), the s-d hybridization is the dominant contribution. Consequently ΔH is relatively insensitive to the bandwidth. In Fig. 4 similar ΔH values are obtained for both a rigid band and a band that narrows as the number of Ni-Ni nearest neighbors decreases. Structural differences enter only indirectly through the changes in hybridization measured in Δh_d. Since the Ni-Al alloys are metallic (and able to screen any charge imbalance), the number of d electrons on a given site and charge neutrality fix the number of s, p electrons associated with that site. These are assumed to occupy a common free electron band shared with the three Al valence electrons. In the spirit of the force theorem, only the kinetic energy of the free electron gas is counted.

As EELS measures the unfilled portion of $d_i(E)$, Friedel's model (and its extension to the alloy) provides a simple framework for interpreting the changes in the Ni $L_{2,3}$ edge, where a smaller white line intensity correlates with increased hybridization and a larger cohesive energy (Fig. 4). From the bulk values of Table I, the d-band filling as a function of Al concentration is $h_d = 1.44(1 - x_{\text{Al}})$. We can then replot Hultgren's measurements to show ΔH [29] vs h_d for intermediate compositions as well as the ordered alloys. We use

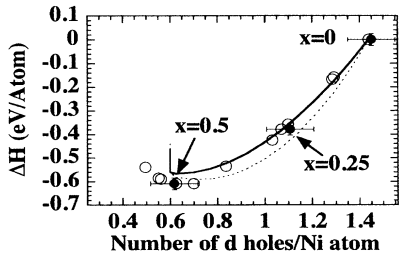

FIG. 4. Correlation between the d-band filling and heat of formation of the bulk alloy $Ni_{1-x}Al_x$. (•) Measured h_d (Table I) vs observed ΔH of [29]; (∘) measured ΔH vs $h_d = 1.44(1 - x)$; (· · ·) modeled ΔH for $W = 3$ eV, $B = 0.25$ eV; (solid line) modeled ΔH with $W = 4 - 2x$ eV, $B = 0.2$ eV.

this phenomenological relationship between h_d and ΔH (Fig. 4) to find the boundary energies γ_B with respect to bulk Ni_3Al (Table I) [30]. ADF images and EDX measurements suggest that large-angle grain boundaries are 2 planes of Ni atoms wide and that the tilt boundaries are half ordered material and half antiphase boundary (APB) (which is 1 plane of Ni atoms wide). The estimates of γ_B from these widths and Fig. 4 are comparable with EAM calculations of other boundary geometries [10].

Ranking the boundaries by γ_B produces an empirical separation into two groups. Those with $\gamma_B \gtrsim 300$ mJ/m^2 are susceptible to environmental embrittlement and intergranular fracture. Those with $\gamma_B \lesssim 300$ mJ/m^2 are not hydrogen embrittled and fracture in a transgranular manner. Lacking more sophisticated models we can estimate only the simplest of these properties, namely, the ideal work of fracture, $\gamma_I = 2\gamma_S - \gamma_B$. The calculated changes in the surface energies γ_S for different surfaces are less than 300 mJ/m^2 [10,31]. This is much smaller than the changes in γ_B for different boundaries so γ_I will be greatest for the smallest γ_B. Using γ_B from Table I, the B-free boundaries are likely to fracture before the bulk fractures while the B-doped boundaries have cohesive energies comparable to the bulk. (This is true only at a Ni-rich boundary; B is unlikely to segregate to an Al-rich boundary [2].) Since pure polycrystalline Ni is ductile, we might suspect that Ni enrichment at grain boundaries in Ni_3Al will impart some ductility to the material. This is the case when the environmental effect is removed [12]. However the fracture mode of the B-free Ni_3Al is still intergranular while B-doped Ni_3Al shows transgranular fracture [12] as would be expected from the above discussion.

It has not escaped our attention that the changes in the measured Ni d-band filling (Fig. 3) also influence the boundary effectiveness in dissociating H_2 [32,33] and the local solubility of atomic H (lower DOS at the Fermi energy correlating with a lower H solubility [34]) and hence provides a likely explanation of the environmental effects. Space limits prevent a full discussion of this here but we note that exposure to H and H_2 (identified as a sources of environmental embrittlement by Liu [13]), might make the B-free boundaries more brittle than the B-doped boundaries, although the microscopic details of the embrittlement process are not obvious.

Our observations of bonding changes due to B doping can, however, account for the change in fracture mode. The success of the simple Friedel model is encouraging; hopefully this will stimulate more rigorous calculations of basic mechanical properties from the measured local electronic structure.

This research was funded by DOE Grants No. DE-FG02-85ER45211 and No. DE-FG02-87ER45322. The Cornell Materials Science Center STEM is operated and acquired through NSF Grants No. DMR-8314255 and No. DMR-9121654.

[1] K. Aoki and O. Izumi, J. Jpn. Inst. Met. **43**, 1190 (1979).
[2] C. T. Liu, C. L. White, and J. A. Horton, Acta Metall. **33**, 213 (1985).
[3] P. E. Batson, Nature (London) **366**, 728 (1993).
[4] N. D. Browning, M. M. Chisholm, and S. J. Pennycook, Nature (London) **366**, 143 (1993).
[5] D. A. Muller *et al.*, Nature (London) **366**, 725 (1993).
[6] S. S. Brenner and H. Ming-Jian, Scr. Metall. **25**, 1271 (1991).
[7] M. K. Miller and J. A. Horton, J. Phys. (Paris) **47**, C7-268 (1986).
[8] J. E. Krzanowski, Scr. Metall. **23**, 1219 (1989).
[9] M. J. Mills, Scr. Metall. **23**, 2061 (1989).
[10] S. M. Foiles, Mater. Res. Soc. Symp. Proc. **81**, 51 (1987).
[11] S. P. Chen *et al.*, Scr. Metall. **23**, 217 (1989).
[12] E. P. George, C. T. Liu, and D. Pope, Scr. Metall. **30**, 37 (1993).
[13] C. T. Liu, Scr. Metall. **27**, 25 (1992).
[14] D. A. Muller and J. Silcox (to be published).
[15] R. D. Leapman, P. Rez, and D. F. Mayers, J. Chem. Phys. **72**, 1232 (1980).
[16] C. Colliex and B. Jouffrey, Philos. Mag. **25**, 491 (1972).
[17] M. Brown, R. E. Peierls, and E. A. Stern, Phys. Rev. B **15**, 738 (1977).
[18] L. F. Mattheiss and R. E. Dietz, Phys. Rev. B **22**, 1663 (1980); T. I. Morrison *et al.*, Phys. Rev. B **32**, 3107 (1985); D. H. Pearson, C. C. Ahn, and B. Fultz, Phys. Rev. B **47**, 8471 (1993).
[19] J. E. Muller and J. W. Wilkins, Phys. Rev. B **29**, 4331 (1984).
[20] D. Hackenbracht and J. Kubler, J. Phys. F **10**, 427 (1980).
[21] J. C. Fuggle *et al.*, Phys. Rev. B **27**, 2145 (1983).
[22] J. Friedel, in *The Physics of Metals,* edited by J. M. Ziman (Cambridge University Press, Cambridge, England, 1969), Sect. 8.2.1.
[23] D. A. Muller and J. Silcox, Philos. Mag. A **71**, 1375 (1995).
[24] D. A. Muller, S. Subramanian, S. L. Sass, J. Silcox, and P. E. Batson, Mater. Res. Soc. Symp. Proc. **364**, 743 (1995).
[25] C. Colinet, A. Bessoud, and A. Pasturel, J. Phys. Condens. Matter **1**, 5837 (1989).
[26] D. G. Pettifor, in *Electron Theory in Alloy Design,* edited by D. G. Pettifor and A. H. Cottrell (Alden Press, Oxford, 1992).
[27] A. Pasturel, P. Hichter, and F. Cyrot-Lackmann, J. Less-Common Met. **86**, 181 (1982).
[28] A. R. Mackintosh and O. K. Anderson, in *Electrons at the Fermi Surface,* edited by M. Springford (Cambridge University Press, London, 1980), Sect. 5.3.
[29] R. Hultgren *et al., Selected Values of the Thermodynamic Properties of Binary Alloys* (American Society for Metals, Metals Park, OH, 1973).
[30] The low energy cost associated with forming a Ni and B-rich grain boundary may seem surprising but is expected since $Ni_{20}Al_3B_6$ precipipates are detected in the bulk for B concentrations exceeding a few thousand ppm [2].
[31] S. M. Foiles and M. S. Dawes, J. Mater. Res. **2**, 5 (1987).
[32] J. Y. Saillard and R. Hoffman, J. Am. Chem. Soc. **106**, 2006 (1984).
[33] B. Hammer and M. Scheffler, Phys. Rev. Lett. **74**, 3487 (1995).
[34] C. D. Gelatt, H. Ehrenreich, and J. A. Weiss, Phys. Rev. B **17**, 1940 (1978).

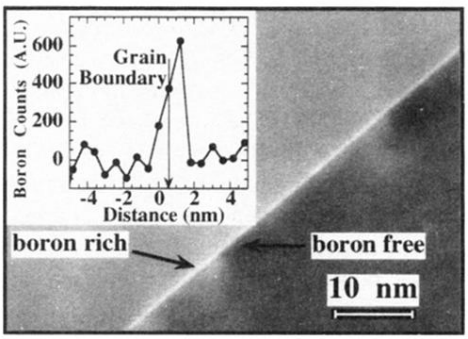

FIG. 2. ADF image of a large-angle grain boundary in B-doped $Ni_{0.76}Al_{0.24}$ (footnote a of Table I). The boundary appears bright due to Ni enrichment. B is present at parts of the boundary which show strain contrast (light). Dark regions have no detectable B. Inset is a EELS B-K edge line scan across the boundary showing B segregation to the boundary.